Cyclic Variability and Dynamical Instabilities in Autoignition Engines with High Residuals

Erik Hellström, *Member, IEEE*, Anna G. Stefanopoulou, *Fellow, IEEE*, and Li Jiang.

***Abstract*—The dynamical phenomenon of cyclic variability in combustion governed by autoignition in homogeneous charge compression ignition (HCCI) engines with large amounts of residual gases is investigated. A novel model is derived with two states that capture the coupling between engine cycles due the thermal energy in the recycled residual gases and the recycled chemical energy in the unburned fuel. With the parameters tuned to data from a single cylinder engine at one level of residuals, the model predictions agree well with the experimental observations of decreasing residuals, which are associated with later phasing and increasing cyclic variability approaching misfire. A stability analysis of the model with respect to the amount of recycled residual gases shows how instabilities develop and that the dynamic behavior of the combustion phasing from cycle to cycle is stable for a range of residual gas fractions. The model and analysis offers an explanation for the experimentally observed cycle-to-cycle variability and provides a foundation for further analysis as well as development of controls mitigating the variability.**

***Index Terms*—Internal combustion engines, nonlinear dynamical systems, Gaussian noise, stability, bifurcation.**

I. Introduction

A high level of residual gas enables lean and efficient combustion based on autoignition of a homogeneous mixture. This combustion mode is called homogeneous charge compression ignition (HCCI), or controlled autoignition, and its low in-cylinder peak temperatures produce very low NO_x emissions which obviate the need for costly exhaust aftertreatment. It was early noted that HCCI combustion can have low cyclic variability (CV) compared to spark ignition (SI) combustion [1]. However, the region with low CV of HCCI is narrow so the feasible operating range is smaller than for SI combustion. In order to satisfy the typical demands of speed and load, frequent transitions to the SI combustion mode would be required. Outside the stable operating range, HCCI combustion can exhibit significant oscillations at late phasing [2]–[4] and increasingly earlier combustion at high loads [5], even though all controllable inputs are held constant. Indeed, at certain operating conditions HCCI combustion phasing can be a) oscillatory, where it alternates between early and late combustion phasing, or b) unstable, where the combustion phasing occurs earlier for every cycle. Oscillatory or unstable combustion phasing has been observed experimentally for HCCI combustion induced by high inlet heating or very high compression ratios [2], [5] and also for HCCI engines with large amounts of internal residual gases [3], [4]. This behavior indicates that there is significant nonlinear coupling between cycles that can stabilize or destabilize the process. The coupling has been attributed to variations from cycle to cycle in combustion inefficiency and residual gas temperature [6], [7] as well as the slower variation in the cylinder wall temperature [5], [8].

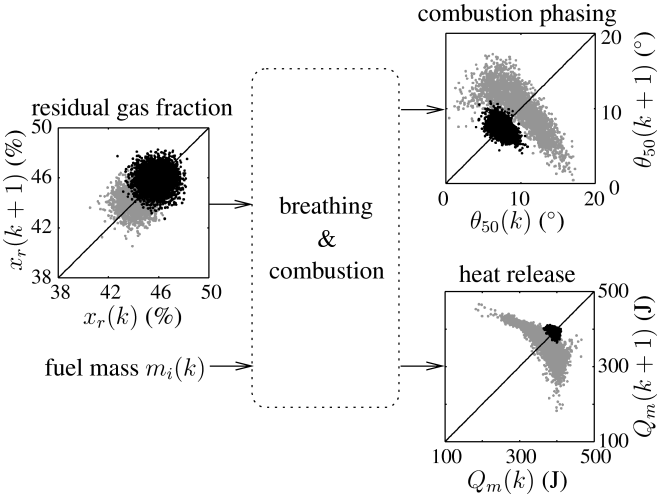

Fig. 1. System overview and experimental return maps for the inputs and the outputs for low CV (black) and high CV (gray). All actuators are held constant in each experiment, the difference between the two cases is different valve timings that changes the average x_r. The characteristic shapes that appear in the return maps are predicted by the physics-based model analyzed here.

The focus of this paper is on the cyclic behavior of lean HCCI. Stoichiometric operation, with spark-assist, shows qualitatively different behavior at conditions with high CV as shown in [9], [10]. Strategies with lower amount of residual gases, such as inlet heating, change the coupling between cycles and, hence, result in different behavior as shown in [11]. Here, lean HCCI combustion with recycling of residuals through negative valve overlap (nvo) is investigated with the aim to understand the dominant dynamical coupling in the process. The dynamics of the combustion is studied as nvo is varied with a fixed injection timing strategy. The considered inputs are the average residual gas fraction, $\bar{x}_r$, and the injected fuel, m_i, see Fig. 1. Through the understanding of these dynamics, model-based cycle-to-cycle control of injection parameters can be subsequently developed for achieving low variability.

Control-oriented models of HCCI combustion have been developed with a few lumped states in [12]–[14]. A one-state temperature model for HCCI with large amounts of residuals was developed in [15] and analysis of the stability was shown

This material is based upon work supported by the Department of Energy (National Energy Technology Laboratory) under award number DE-EE0003533.

E. Hellström and A. G. Stefanopoulou are with the Department of Mechanical Engineering, University of Michigan, Ann Arbor, MI USA (e-mail: {erikhe,annastef}@umich.edu). L. Jiang is with Robert Bosch LLC, Farmington Hills, MI USA (e-mail: li.jiang@us.bosch.com).

in [16]. The nonlinear coupling between the temperature at the beginning of the cycle and the residual temperature allowed the prediction of unstable behavior with limit cycles at late phasing and thermal runaway at early phasing. Similar analysis is shown in [17] and used in [18] to develop a switched linear model. Common among all these models of varying order is the nonlinear coupling due to the cylinder temperature evolution and the autoignition based on an Arrhenius expression.

Reducing CV by controlling the fuel injection during the nvo period is investigated experimentally in [19], [20] for extending the low load limit of HCCI. Linear controllers for reducing CV are developed in [21], [22] using variable valve timing and in [23] using fuel injection timing. The control is based on models where complete combustion is assumed and the linearization predicts that the trend at late phasing is that one cycle with early combustion phasing is followed by a late cycle and conversely. For conditions with higher CV at late phasing the relationship between cycles is clearly nonlinear and a linear correlation between cycles does not capture the experimentally observed patterns. This behavior is mainly due to the sharp falloff in the combustion efficiency for late phasing as shown in [4], [24]. As a consequence, the unburned fuel mass creates an important coupling between cycles in addition to the residual gas temperature. A two-state model including the evolution of temperature and fuel mass was therefore derived in [25]. This model is here examined by studying the stability through bifurcation analysis and numerical simulations using physically reasonable parameters. It is shown that the onset of instability is predicted by the analysis and that by adding stochastic noise to one of the model inputs, the dynamic evolution seen in experiments for conditions with progressively higher CV approaching misfire is predicted.

Misfire in HCCI is studied in simulation using models including chemical kinetics and gas flows in [26] and using a simplified eight-state model in [27]. The approach followed here includes only the dominating mechanisms of temperature and unburned fuel as identified through the experiments in [4], [6], [24]. The two state model is still capable of predicting misfires and is amendable for analysis as well as suitable for future control of the nvo and cycle-to-cycle fuel injection for reducing CV.

The feedback from the residual gas also plays an important role in SI engines where this coupling can give high CV. Dynamical instabilities for a one-state temperature model of SI combustion were studied by Kantor [28] and lean SI operation was modeled and analyzed by Daw et al. [29] using a two-state model where parametric uncertainties were introduced as stochastic noise. Although SI combustion is clearly distinct from HCCI, our approach is inspired by these works. Specifically, our aim is to formulate and analyze low-order descriptions of the main dynamical couplings and we utilize white noise to model fluctuations of the residual gas fraction around the controllable mean value.

The paper is organized as follows. The HCCI combustion process is introduced first with an overview and some experimental observations. The combustion model, with temperature and fuel states, is described in Sec. III and validated in Sec. IV. After that, the stability of the second-order model is studied.

II. System overview

In this work, HCCI combustion is induced by closing the exhaust valve early creating a so-called negative valve overlap where significant amounts of hot residuals are trapped and undergoes another compression and expansion [30]. The dilution, the residual gas fraction x_r, strongly affects the combustion, mainly since autoignition is very sensitive to the thermal conditions. The level of x_r depends on the thermodynamic process in a complicated way but is mainly controlled by the nvo for naturally aspirated HCCI engines, which are studied here. The injected fuel mass m_i is typically used to regulate the load but can be used in the future to also reduce the CV as it influences the combustion phasing and it can be modified from cycle to cycle. Note here that the injection timing could also be used, although the model presented here does not capture the effect of injection timing. The control authority in combustion phasing is inherently limited using injection parameters whereas it is large using nvo to manipulate x_r. At the same time, the control of x_r is considerable slower with commercially viable cam phasing mechanisms.

The combustion process can be described by the heat release as a function of the crank angle. A common measure of the combustion phasing is the 50% burn angle, where half the total heat release occurred, since it is rather robust against measurements noise due to the very rapid nature of HCCI combustion [31]. Therefore, the 50% burn angle, denoted by θ_{50}, is an important variable for feedback control of the combustion and the dynamics of θ_{50} is the main focus of the study. For conditions with high CV the heat release may vary significantly between cycles despite constant fueling due to highly varying combustion efficiency [4]. To show these dynamics, the total heat release, denoted by Q_m, is also studied. The complete input–output view is shown in Fig. 1 together with experimental data for two operating conditions.

The return maps for the input and output in Fig. 1 show the relationship between subsequent values of the variables and are acquired with the valve timings set for different nvo. The valve timings affect the mean value of x_r from 46% (black dots) to 44% (gray dots). The successive cycle-to-cycle values of x_r are assumed uncorrelated in both cases, as indicated by the return maps for x_r. However, the relationship between successive cycle-to-cycle values of the outputs changes notably when reducing the mean x_r. As seen in Fig. 1, the experimental output for the low CV case (black dots) do not show any strong correlation whereas in the high CV case (gray dots) characteristic shapes appear in the return maps which indicate low-order deterministic couplings between consecutive cycles. These characteristics are typical for the experimental findings [4] and they get more pronounced as the CV increases. The experimental results in Fig. 1 suggest that a bifurcation occurs when reducing x_r where the term bifurcation is used in the general sense meaning that the dynamical behavior changes qualitatively. The result of this work is the formulation and analysis of low-order models that can predict the main features seen in experiments thereby offering an explanation for and a way to analyze the cyclic variability.

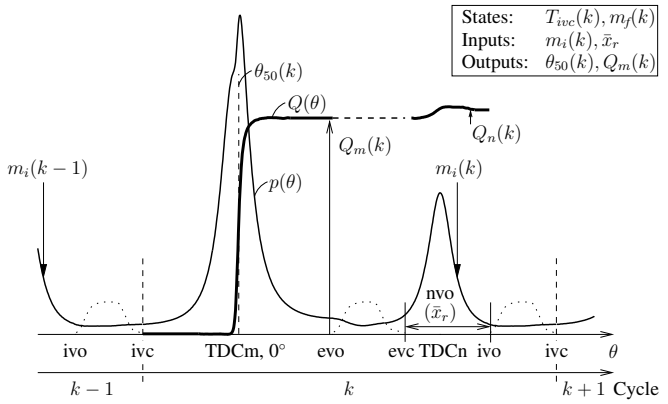

Fig. 2. Definition of the engine cycle and important variables for typical cylinder pressure $p(\theta)$, heat release $Q(\theta)$, and valve lift (dotted line).

III. Combustion model

A natural choice of model states of a low-order model are the temperature $T_{ivc}(k)$ at intake valve closing (ivc) and the fuel amount $m_f(k)$ in the beginning of cycle k. The inputs are the injected fuel mass $m_i(k)$ and the mean residual gas fraction $\bar{x}_r$. The definition of the engine cycle and important variables in the model are shown in Fig. 2. In the following sections, the second-order model is derived. The modeling approach is based on first principles and only considers the dominating mechanisms so that the experimental observations are reasonably predicted, which is indeed the case as shown in Sec. IV, with a simple model amenable for analysis and control design.

A. Fuel dynamics

The fuel mass at ivc $m_f(k)$ of cycle k is

$$m_f(k) = m_i(k-1) + m_u(k) \tag{1}$$

where $m_i(k-1)$ fuel mass injected in the preceding nvo period, see Fig. 2, and $m_u(k)$ is the unburned fuel mass carried over from previous cycles. During main combustion, the fraction η_m of $m_f(k)$ is consumed and, during the nvo period, the fraction $x_r(k)$ of the residual gases is trapped. With homogeneously mixed residuals, then

$$m_f(k)\,(1-\eta_m)\,x_r(k) \tag{2}$$

is present at the beginning of the nvo. The fraction η_n is further consumed during nvo so the unburned fuel carried over to the next cycle is

$$m_u(k+1) = m_f(k)\,(1-\eta_m)\,x_r(k)\,(1-\eta_n) \tag{3}$$

where η_m is a function of end of main combustion θ_m and η_n is a constant as described in the next section. The fuel mass dynamics is thus

$$\begin{aligned} m_f(k+1) = {} & m_i(k) + \\ & x_r(k)\,(1-\eta_m(\theta_m))\,(1-\eta_n)\,m_f(k) \end{aligned} \tag{4}$$

obtained from Eq. (1) and (3).

B. Heat release

The crank angle timing of the main combustion is given by an Arrhenius expression whereas the timing for the combustion during re-compression is constant. The ignition delay for the main combustion is given by

$$\tau = Ap(\theta)^n \exp\big(B/T(\theta)\big) \tag{5}$$

with the tuned parameters (A, B, n) [13], [32]. The pressure $p(\theta)$ and temperature $T(\theta)$ are given by polytropic processes, see Eq. (15a) in Sec. III-C, with the exponent m. The start of combustion is given by $\theta_{soc} = \kappa^{-1}(1)$ where

$$\kappa(\theta_{soc}) = \int_{\theta_{ivc}}^{\theta_{soc}} \frac{dt}{\tau}, \quad dt = d\theta/\omega \tag{6}$$

and ω is the engine speed [33]. The end of the main combustion θ_m is given by

$$\theta_m = \theta_{soc} + \Delta\theta, \quad \Delta\theta = d_1\theta_{soc} + d_0 \tag{7}$$

where $\Delta\theta$ is the burn duration and (d_0, d_1) are tuned parameters. The complete ignition model becomes

$$\theta_m(T_{ivc}) = \kappa^{-1}(1)\,(1+d_1) + d_0 \tag{8}$$

implicitly defined by Eq. (5)–(7). The combustion phasing, the 50% burn angle, is one output from the model and is given by

$$\theta_{50} = \theta_{soc} + \Delta\theta/2. \tag{9}$$

The temperature rises due to combustion are assumed to occur instantaneously at θ_m, given by (7), and θ_n, which is assumed constant, and given by

$$\Delta T_m = \frac{Q_{nm}}{c_v m_t}, \quad \Delta T_n = \frac{Q_{nn}}{c_v m_t x_r} \tag{10}$$

where m_t is the charge mass, given later in Eq. (21), and $m_t x_r$ is the residual charge mass. Assuming that sufficient oxygen is present (lean combustion), the net heat of reaction during main combustion Q_{nm} is modeled by

$$Q_{nm} = m_f \eta_m(\theta_m) q \tag{11}$$

where m_f is the fuel mass, η_m is the combustion efficiency, and $q = q_{lhv}(1-\epsilon)$ where q_{lhv} is the lower heating value and ϵ represents heat losses. At exhaust valve closing (evc), the fuel mass is given by Eq. (2) and the net heat release during the nvo Q_{nn} is then

$$Q_{nn} = m_f(1-\eta_m(\theta_m))x_r\eta_n q \tag{12}$$

where η_n is the combustion efficiency of the re-compression phase.

The completeness of the main combustion, captured by the efficiency η_m, is modeled as a sigmoid function of θ_m as

$$\eta_m(\theta_m) = e_1\left(1 + \exp\frac{\theta_m - e_2}{e_3}\right)^{-1} \tag{13}$$

which captures the trend in experimental data [4]. The dependence of η_m on the combustion phasing was identified in [4] as one key nonlinearity for describing the behavior at high CV while no clear trends were observed for the efficiency of the nvo period η_n. For simplicity, η_n is assumed constant.

C. Temperature dynamics

By assuming adiabatic mixing of ideal gases with constant specific heats, the temperature at ivc $T_{ivc}(k+1)$ of cycle $k+1$ is given by

$$T_{ivc}(k+1) = (1 - x_r(k))T_{im} + x_r(k)T_r(k) \tag{14}$$

where $x_r(k)$ is the residual gas fraction and T_{im} is the intake manifold temperature which is considered fixed. The temperature of the intake is varying slowly relative to the duration of an engine cycle and is typically close to ambient temperature. The temperature of the residual gas $T_r(k)$ of cycle k is derived in the following.

The compression and expansion are polytropic processes with slope γ, which for simplicity is assumed constant. The pressure and temperature are thus given as a function of crank angle θ by

$$\left.\begin{aligned} p(\theta) &= p_{ivc}\left(\frac{V_{ivc}}{V(\theta)}\right)^{\gamma} \\ T(\theta) &= T_{ivc}\left(\frac{V_{ivc}}{V(\theta)}\right)^{\gamma-1} \end{aligned}\right\} \text{ if } \theta \in (\theta_{ivc}, \theta_m] \tag{15a}$$

$$\left.\begin{aligned} p(\theta) &= p_{am}\left(\frac{V(\theta_m)}{V(\theta)}\right)^{\gamma} \\ T(\theta) &= T_{am}\left(\frac{V(\theta_m)}{V(\theta)}\right)^{\gamma-1} \end{aligned}\right\} \text{ if } \theta \in (\theta_m, \theta_{evo}] \tag{15b}$$

where $V(\theta)$ is the cylinder volume function given by Eq. (27) and $V_x = V(\theta_x)$ is the volume at the crank angle θ_x. It is assumed that the combustion occurs instantaneously at θ_m, given by (8), and the state after combustion is given by

$$T_{am} = T(\theta_m) + \Delta T_c, \quad p_{am} = p(\theta_m)\frac{T_{am}}{T(\theta_m)} \tag{16}$$

where ΔT_c is given by (10).

The blowdown occurs instantaneously and the remaining gases follow a polytropic process from pressure at exhaust valve opening $p(\theta_{evo})$ to exhaust manifold pressure p_{em}

$$T_{bd} = T_{evo}\left(\frac{p_{em}}{p(\theta_{evo})}\right)^{1-1/\gamma} \tag{17}$$

and the temperature of the residual gases at exhaust valve closing becomes

$$T_{evc} = c_e T_{bd} \tag{18}$$

where c_e accounts for cooling of the residuals during the exhaust process.

The compression and expansion during nvo are polytropic processes, thus $p(\theta)$ and $T(\theta)$ are given by expressions analogous to Eq. (15a) for $\theta \in (\theta_{evc}, \theta_n]$ and Eq. (15b) for $\theta \in (\theta_n, \theta_{ivo}]$. The state after instantaneous combustion of the unburned fuel at θ_n, which is assumed constant, is given by

$$T_{an} = T(\theta_n) + \Delta T_r, \quad p_{an} = p(\theta_n)\frac{T_{an}}{T(\theta_n)} \tag{19}$$

where ΔT_r is given by (10). Finally, the temperature of the residual gases at intake valve opening is formulated based on the temperature T_{ivo} obtained after polytropic expansion from T_{an}:

$$T_r = T_{ivo} = T_{an}\left(\frac{V(\theta_n)}{V_{ivo}}\right)^{\gamma-1} \tag{20}$$

Now, express the charge mass as

$$m_t = \frac{p_{ivc}V_{ivc}}{RT_{ivc}} \tag{21}$$

and introduce the following parameters

$$\alpha = c_e\left(\frac{p_{em}}{p_{ivc}}\right)^{\frac{\gamma-1}{\gamma}}\left(\frac{V_{evc}}{V_{ivo}}\right)^{\gamma-1} \tag{22a}$$

$$\beta = \frac{q(\gamma-1)}{p_{ivc}V_{ivc}^{\gamma}} \tag{22b}$$

$$\zeta = \frac{q\eta_n(\gamma-1)}{p_{ivc}V_{ivc}V_{ivo}^{\gamma-1}}V(\theta_n)^{\gamma-1} \tag{22c}$$

which are assumed constant for a given operating condition. By combining Eq. (10)–(12) and (15)–(21) this parametrization gives the following description for the temperature of the residual gases at the end of cycle k:

$$T_r(k) = \Big\{\alpha\left[1 + \beta\eta_m(\theta_m)m_f(k)V(\theta_m)^{\gamma-1}\right]^{\frac{1}{\gamma}} + \zeta m_f(k)(1-\eta_m(\theta_m))\Big\}T_{ivc}(k) \tag{23}$$

where $\theta_m = \theta_m(T_{ivc}(k))$ is given by (5)–(7). The parameter α is related to the engine breathing, through the ratio p_{em}/p_{ivc} of exhaust to ivc pressure, and the exhaust process, by the cooling factor c_e (note that $V_{evc}/V_{ivo} \approx 1$ since nvo typically is close to symmetrical). The β and ζ are related to the temperature rise per mass of fuel that burns during the main combustion and during the re-compression, respectively.

D. Residual gas fraction

The level of the residual gas fraction x_r is regulated by the nvo but analysis of estimates of x_r for different nvo settings in [4] shows that nvo only controls the mean value $\bar{x}_r$, see also the return map for x_r in Fig. 1. The variations around the mean are shown to be close to normally distributed with a standard deviation of approximately 0.8%. Thus, there are almost no deterministic relationships between subsequent values and to capture the apparent randomness, x_r is modeled as a constant $\bar{x}_r$ with added Gaussian white noise,

$$x_r(k) = \bar{x}_r + e(k), \quad e(k) \in N(0, \sigma) \tag{24}$$

where $e(k)$ is normally distributed with zero mean and variance σ^2. The properties of $x_r(k)$ are estimated from experiments but the modeling approach can also be interpreted as treating higher order dynamical effects as stochastic noise from many sources so that their combined effect is approximately normally distributed, see [29] where stochastic noise is used to account for parametric uncertainties in a model for lean SI operation. Underlying physical phenomena may, e.g., be due to turbulent flow that affects the amounts of residuals from one cycle to the next.

E. Complete model

The temperature at ivc and the fuel mass in the next cycle $k+1$ are given by the states at cycle k and the inputs, $m_i(k)$ and $\bar{x}_r$,

$$\begin{cases} T_{ivc}(k+1) = f\left(T_{ivc}(k), m_f(k), x_r(k)\right) \\ m_f(k+1) = g\left(T_{ivc}(k), m_f(k), m_i(k), x_r(k)\right) \end{cases} \quad (25)$$

where $x_r(k)$ is given by (24), f is defined by (14) and (23), and g is defined by (4). The outputs are

$$\begin{cases} \theta_{50}(k) = h(T_{ivc}(k)) \\ Q_m(k) = m_f(k) q_{lhv} \eta_m(\theta_m(T_{ivc}(k))) \end{cases} \quad (26)$$

given by (8), (9), and (13). Compared to related work, such as [12]–[17], the state-dependent efficiency $\eta_m(\theta_m(T_{ivc}(k)))$, the term with the parameter ζ, and the parameter η_n in Eq. (4) and (23) are the important differences since these represent the effect of incomplete combustion, heat release during re-compression, and recycled unburned fuel. In particular, the one-state model in [15] is obtained by letting $\eta_m = \eta_n = 1$, $\zeta = 0$, and $V_{evc}/V_{ivo} = 1$. In a study of spark-assisted HCCI [34], the unburned fuel mass is estimated based on a model that can be derived from Eq. (3), (11), and (12) if the heat release during the nvo period is neglected which implies letting Q_n and η_n be zero. In summary, the developed model compared to these previous low-order models [12]–[17], [34] captures the coupling introduced by the unburned fuel mass that has been identified as an important mechanism, in addition to charge temperature, for explaining the high CV [4]. In comparison with higher fidelity models, such as [26] and [27], the developed second-order model (25) captures the main mechanisms and is more amenable for nonlinear control development. It can finally be noted that all the previously mentioned HCCI models are deterministic while the model of the residual gas fraction (24) introduces a stochastic element, which is essential in order to reproduce the dynamic evolution observed in experiments as shown in the remainder of this paper.

IV. Model validation

Experiments to tune and validate the proposed model were performed at the Automotive Laboratory at University of Michigan on a single-cylinder gasoline direct-injection engine with a Ricardo Hydra crankcase. The displacement is 0.55 L, the compression ratio is 12.5, and the engine is equipped with a fully-flexible valve actuation system. More details on the setup are found in [35]. The fuel is research grade gasoline and is delivered in one injection during nvo starting at 330° before the top dead center of the main combustion (TDCm). The experiments were run in open loop with all actuators constant except for coolant control and the dynamometer keeping the speed constant at 2000 rpm. Nominal conditions represent a typical medium load operation point where the injected fuel mass m_i is 9.6 mg/cycle corresponding to 2.8 bar net indicated mean effective pressure (IMEP) and relative air-fuel ratio $\lambda = 1.7$.

To fully observe the dynamical evolution, data for 3000 engine cycles were recorded in each operating point which is about ten times more cycles than for a typical experiment.

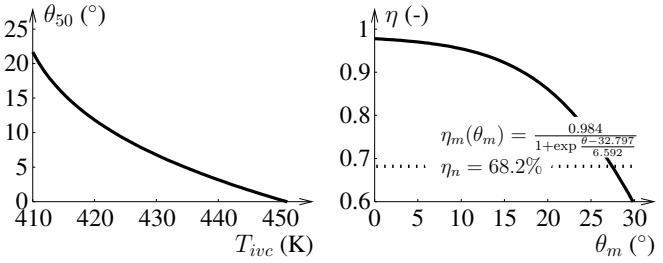

Fig. 3. Left: The model for ignition timing. Right: The efficiency model.

For the analysis, the engine data are subsequently processed by an iterative procedure to calculate important variables for each individual cycle. This procedure includes residual gas fraction estimation, gross heat release analysis, and estimation of unburned fuel and combustion efficiencies. More details on the estimation procedure are found in [4], [25].

A. Parametrization

The parameters of the model described by (4), (14), and (23) are determined from sensor readings, data sheets, and data fitting as described in the following. The data used for fitting are taken from an operating condition with fairly high CV. The coefficient of variation (standard deviation divided by sample mean), CoV, of IMEP is 13.3% whereas, in production engines, an acceptable level is below 5%. This was a deliberate choice to get sufficiently rich data for capturing the evolution at high CV. With the parametrization described next, the model captures that the couplings between cycles change as the internal dilution varies and cause the CoV to vary from 2.4% to 17.8%.

The operating conditions, obtained from the sensor measurements, are shown in Tab. I. For the model of the cylinder volume, the engine geometry is 0.55 L displacement per cylinder and a compression ratio r_c of 12.41:1. The bore b is 86 mm and the stroke $2a$ is 94.6 mm while the connecting rod length l is 156.5 mm. With these parameters, the volume V at the crank angle φ is obtained by

$$V = \frac{\pi a b^2}{4}\left(1 + l/a + \frac{2}{r_c - 1} - \cos\varphi - \sqrt{(l/a)^2 - \sin^2\varphi}\right) \quad (27)$$

from the standard relations, see [36, Ch. 2.2].

The parameters for the ignition model (8) are fitted to data by interpreting the start of combustion θ_{soc} as the 10% burn angle and θ_m as the 90% burn angle. The values are given in Tab. II and the relationship between θ_{50} and T_{ivc} is depicted in the left panel of Fig. 3. The efficiency model for the main combustion $\eta_m(\theta_m)$ in Eq. (13) and the constant efficiency of the nvo combustion η_n are fitted to data. The efficiency models are depicted in the right panel of Fig. 3.

The lumped temperature parameters α and β are computed from (22a) and (22b), respectively, whereas ζ was increased from its nominal value, given by (22c), manually in order to roughly tune the predicted onset of the instabilities, discussed in Sec. V, to match the data. The values are given in Tab. III.

In summary, the parameters that typically are not known or measured on-board are the 6 parameters for the combustion phasing in Tab. II, the 4 parameters for the temperature

TABLE I
OPERATING CONDITIONS.

Parameter	Symbol	Value
Engine speed	ω	2000 rpm
Intake valve closing	ivc	203 °aTDCn
Pressure at ivc	p_{ivc}	1.09 bar
Intake temperature	T_{im}	313 K

TABLE II
IGNITION DELAY AND BURN DURATION CHARACTERISTICS.

Parameter	Symbol	Value
Scaling factor	A	0.2865 $^{s}/_{\text{bar}^n}$
Temperature factor	B	$7.974{\cdot}10^3$ K
Pressure exponent	n	-4.337
Polytropic exponent	m	1.303
Burn duration offset	d_0	7.574° aTDCm
Burn duration slope	d_1	1.488

TABLE III
LUMPED PARAMETERS FOR THE TEMPERATURE DYNAMICS.

Parameter	Symbol	Value
Breathing parameter	α	0.773
Temperature rise factor, main comb.	β	1.819 $^{l}/_{\text{mg m}^{3(\gamma-1)}}$
Polytropic exponent	γ	1.309
Temperature rise factor, nvo comb.	ζ	0.127 $^{l}/_{\text{mg}}$

evolution in Tab. III, and the 4 parameters for the efficiency models in the right panel of Fig. 3. Additional work is needed in the future to tune these parameters systematically for different engine operating conditions.

B. Comparison with experiments

Model predictions for varying nvo are generated by feeding the model (25) with $x_r(k)$ according to (24) by generating samples from a normal distribution with different $\bar{x}_r$. The mean value $\bar{x}_r$ is set equal to the mean value estimated for each experimental condition. The fuel input m_i is set to the measured value 9.6 $^{\text{mg}}/_{\text{cycle}}$. All model parameters are constant for all the evaluated cases and have been tuned to match the case for nvo = 147°. The initial conditions $T_{ivc}(0), m_f(0)$ for the model are unknown. These are guessed and the model is iterated a large number of times and the initial transients are removed. After that 3000 samples are recorded (the same number as in the experiments).

The return maps from experimental measurements and predicted by the model are shown in Fig. 4 and 5 for the outputs (26), combustion phasing and heat release during main combustion. The experimental return maps immediately show nonlinear dynamical features. The behavior changes notably, in a qualitative sense, when reducing the nvo which mainly reduce the mean of the almost normally distributed residual gas fraction x_r, see Fig. 1. Further, the characteristic patterns that emerge are asymmetric about the diagonal implying asymmetry in time. This means that it cannot be described by any one-to-one transformation of a stationary Gaussian random process [37, Thm. 1].

The measured and predicted patterns for the phasing θ_{50} have one part, or "leg", that stretches out approximately perpendicular to the diagonal. For low x_r another "leg" appears for low $\theta_{50}(k)$ in the left part of the figure bending the left tip of the pattern. The angle between the emerging main leg

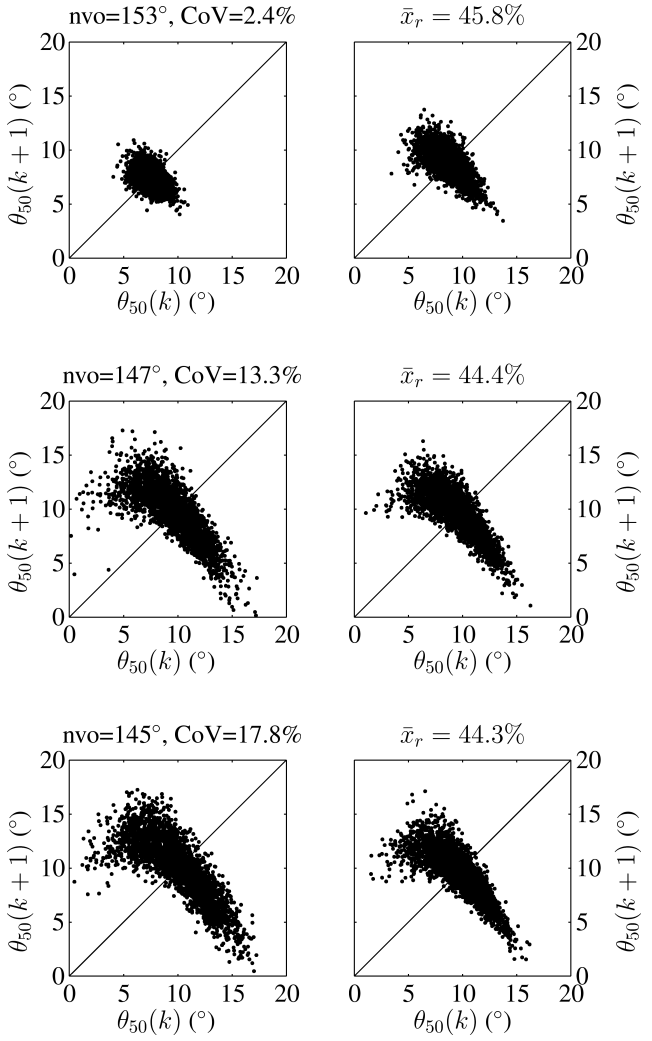

(a) Measurements. (b) Predictions.

Fig. 4. Measured and modeled return maps for the combustion phasing of the main combustion $\theta_{50}(k)$ for decreasing nvo, which decreases the average residual gas fraction $\bar{x}_r$ and increases the CoV of IMEP. The operating condition is 2000 rpm and 2.8 bar IMEP.

and the diagonal is approximately -1 indicating that unstable behavior with increasing oscillation amplitude occurs. The bent tip shows that there is a limit so that when the amplitude gets sufficiently large, the combustion recovers and the oscillation amplitude will reduce in the following cycle.

The total gross heat release during main combustion Q_m shows an emerging pattern that can be described as three "legs" that stretch out in different directions from the middle of the cloud. The two most apparent ones are pointing vertically and at the upper left corner. The smaller third leg is pointing almost parallel to the diagonal. The vertical leg indicates an unstable behavior where, for an average heat release around 400 J, the following cycle can have a large range of heat release values. These legs indicate sequences of cycles starting far down the vertical that is followed by a lower heat release and then a higher than average before returning to closer to average values.

The second-order model is a considerable simplification of the complex phenomena in the combustion process with the parameters tuned for one case and thus some discrepancies

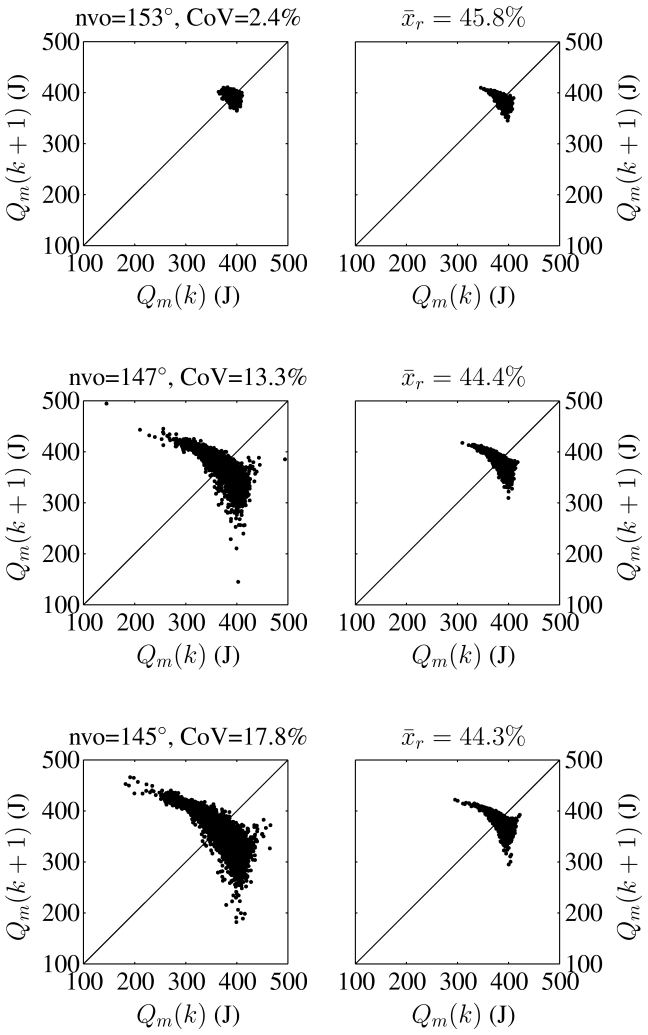

(a) Measurements. (b) Predictions.

Fig. 5. Measured and modeled return maps for the total gross heat release during the main combustion $Q_m(k)$ for decreasing nvo, which decreases the average residual gas fraction $\bar{x}_r$ and increases the CoV of IMEP. The operating condition is 2000 rpm and 2.8 bar IMEP.

are expected. The most apparent differences between the measurements and the predictions are the smaller thickness of the predicted heat release return map and the overestimated level of variability in the first case. Still, there are good geometric similarities between the patterns that emerge when gradually proceeding from a low to a high variability case. The different directions, or "legs", that appear in the return maps are getting more pronounced as x_r decreases, and CoV IMEP increases, and this is captured well by the model.

C. Remarks

Other operating conditions at lower and higher load were also analyzed, which showed that the same characteristics appear with the addition of runaway phenomena at higher loads. Moreover, analogous experiments investigating high CV were performed on a four-cylinder 2 L engine in [24] and compared to data from the single-cylinder used here. The analysis in [24] shows that the dynamical evolution of the combustion phasing θ_{50} is qualitatively similar between the single-cylinder and the individual cylinders on the multi-cylinder engine. The agreement between different engine platforms supports that the dynamical evolution of θ_{50} is indeed a general characteristic of lean HCCI operating with high residuals. It also means that the model developed here can capture the behavior in a multi-cylinder engine, possibly utilizing cylinder-individual values $\bar{x}_r$ and a few parameters.

V. Analysis of temperature and fuel dynamics

The stability of the model is first investigated through a bifurcation analysis on the underlying deterministic model in Eq. (25)–(26) by assuming that the residual gas fraction $x_r(k)$ is constant. After that, numerical simulations show the dynamical behavior of the complete model with noise when $x_r(k)$ is described by Eq. (24).

A. Bifurcation diagram

Bifurcation diagrams are constructed with residual gas fraction x_r as the bifurcation parameter and the injected fuel mass m_i constant. Accordingly, the curve of fixed points (equilibrium points) $x^*(x_r)$ defined by

$$x^* = F(x^*; x_r)$$

is sought where the map F is given by Eq. (25) as

$$x(k+1) = F(x(k); x_r) = \begin{bmatrix} f\left(T_{ivc}(k), m_f(k), x_r\right) \\ g\left(T_{ivc}(k), m_f(k), m_i, x_r\right) \end{bmatrix}$$

where $x(k) = [T_{ivc}(k), m_f(k)]$, f is defined by (14) and (23), and g is defined by (4). The problem of finding the curve of fixed points to a map can be solved with numerical continuation techniques and a predictor-corrector method based on the Moore-Penrose matrix pseudo-inverse is used here, see [38, Ch. 10]. The linear stability of a fixed point is determined by numerically estimating the Jacobian $F_x(x^*; x_r)$ and computing its eigenvalues μ, which are called multipliers. The stability of a cycle of period n is determined analogously by studying the composition of the map n times, e.g., $F(F(x^*; x_r); x_r)$ for $n = 2$. The fixed point curve is finally transformed with the output equations (26) to produce the diagrams in Fig. 6. It is concluded from these diagrams that at x_r of 44% an instability occurs, a one-dimensional bifurcation with one stable multiplier and the other at -1, and a stable period-2 cycle appears. More period-doubling bifurcations occur with shorter intervals for lower x_r, the first is the stable period-4 cycle at 41.6%. For increasing residual gas fraction, the stability is lost at x_r of 60%, see Fig. 6, and the model predicts a thermal runaway where the phasing gets increasingly advanced. In reality the acceptable ringing of the engine would probably limit the operation, before runaway occurs, to a phasing after TDC and thus less than x_r of 56% in this case.

In Fig. 7, the stable fixed points for cycles of periods 1,2,4,8 are shown in return maps. When x_r is reduced towards 40%, a behavior resembling chaos appears and the iterates of the model fall on the attractors shown with small dots in the figure. These curves for the lowest x_r are almost one-dimensional which means that given the value in one cycle, a simple one-dimensional function can predict a value in the next cycle

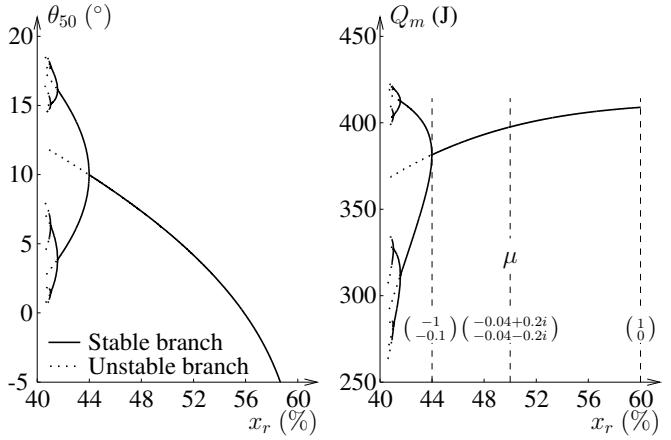

Fig. 6. Bifurcation diagrams for the combustion phasing θ_{50} and the gross heat release during main combustion Q_m for the two-state model (25) with varying residual gas fraction x_r. The value of the multiplier μ is also shown. Period-doubling bifurcations occur when x_r is decreased below 44% and thermal runaway occurs when x_r is increased towards 60%.

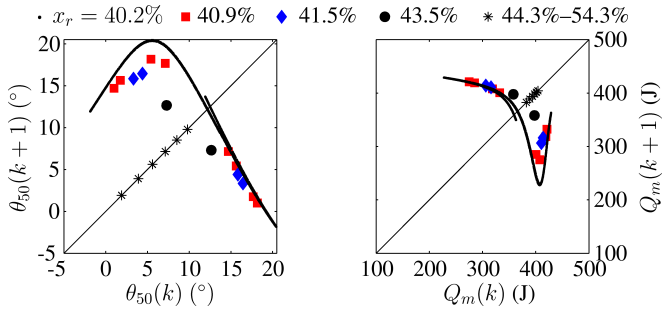

Fig. 7. Behavior of the model for x_r between 40.2% and 54.3%. The stars ($*$) show stable fixed points and the symbols ($\bullet, \blacklozenge, \blacksquare$) show stable cycles of period (2,4,8). The dots ($\cdot$) show 3000 iterates of the model for x_r of 40.2%.

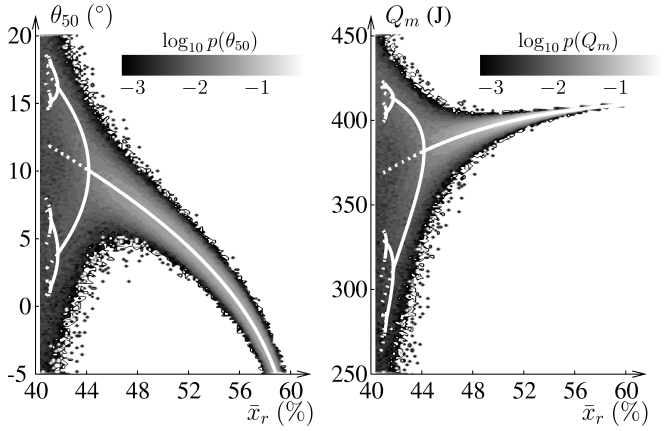

Fig. 8. The noisy orbit diagram is visualized by the probability distribution for the outputs (in scales of gray). Overlaid are the bifurcation diagrams (in white) from Fig. 6.

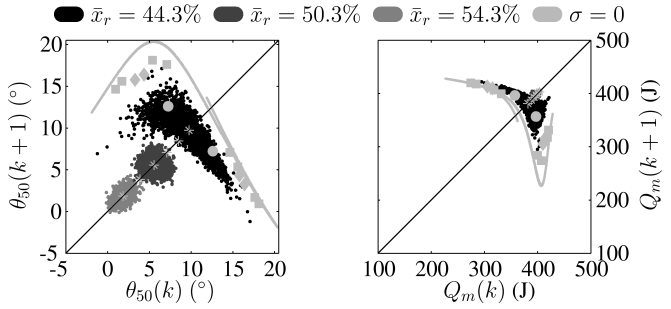

Fig. 9. Noisy return maps for varying $\bar{x}_r$ (black). The noise-free behavior (σ = 0) from Fig. 7 is also shown (bright gray). For $\bar{x}_r$ = 44.3% the deterministic model is stable and close to a period-2 cycle, with stochastic input the behavior changes notably. When $\bar{x}_r$ is increased towards the early instability, a positive correlation between successive θ_{50} appears.

for these conditions. However, if the dynamic behavior is chaotic then nearby trajectories diverge fast and only short term prediction of a few cycles can be expected. Moreover, in reality for these extremely low values of x_r there is a risk for combustion so irregular that the engine stalls.

B. Orbit diagram with noise

The bifurcation analysis in the previous section studies the stability as the parameter x_r is varied between different constant values. As explained above, x_r is more accurately described as the random process in Eq. (24). Dynamical systems close to bifurcation points may, in general, have different behavior for time-varying versus constant parameters, see the discussion and examples in [39, Ch. 3.3]. The effect of the variability in x_r is investigated as follows. The outputs (26) from the nonlinear deterministic model (25) become random processes when using the input model (24). To study the characteristics of the output the model is iterated 3000 times, discarding initial transients, for varying $\bar{x}_r$. The value of σ is 0.8% and m_i is at the constant value of 9.6 mg/cycle, these values correspond to the experimental conditions described in Sec. IV. The characteristics of the generated time-series are discussed in the following.

The calculated probabilities for combustion phasing and heat release in the time series for each $\bar{x}_r$ are shown in Fig. 8. Also shown are the (noise-free) bifurcation diagrams from Fig. 6. The diagram shows that the output variance increases as $\bar{x}_r$ reduces and it is possible to discern that the probability distribution tends to develop from a uni-modal shape to more of a bi-modal as $\bar{x}_r$ reduces below the value of the first period-doubling. However, the fine structure of the bifurcation diagram is no longer visible with this level of noise.

The return maps for $\bar{x}_r$ of 44.3%, 50.3%, and 54.3% are shown in Fig. 9 overlaid with the noise-free return maps from Fig. 7. For the late phasing point with $\bar{x}_r$ = 44.3%, the corresponding noise-free behavior is a stable fixed point although close to the period-2 cycle appearing at 44.0%. With noise, a complex behavior appears which is a result of the nonlinear deterministic model filtering the Gaussian white noise process. Through this filtering, deterministic couplings between cycles are introduced that, in the return maps, manifest as distinct patterns. For $\bar{x}_r$ = 50.3% the multipliers μ are close to the origin (see Fig. 6), the system dynamics is well damped, and the noisy return map for θ_{50} becomes a featureless cloud. As $\bar{x}_r$ is increased and θ_{50} becomes earlier, the point of thermal runaway is approached and a positive correlation between successive θ_{50} appears in the noisy return map. For these early conditions, the variation in Q_m is low due to consistently high combustion efficiency. In summary, the results in Fig. 9 suggest

qualitatively different dynamical behavior when the average phasing is late, normal, and early. In the first case, there are oscillations between early and late phasing with amplitude that is limited by the bent tip of the pattern. For normal phasing, the variations between cycles appear to be random while the positive correlation for higher $\bar{x}_r$ suggests sequences where the phasing increases from one cycle to the next.

The attractors in the noise-free case for x_r = 40.2% have similar shapes but do not have the same level of agreement as the noisy return maps, see Fig. 8–9. Note that the deterministic model still has a stable cycle (period 8) at 40.9% which is more than 4σ from $\bar{x}_r$ = 44.3% (the lowest $\bar{x}_r$ in Fig. 4) which means that the samples of x_r are very rarely in the region where the model may exhibit chaotic behavior (with a constant x_r). Thus, the nonlinear deterministic model driven with stochastic input offers a reasonable description of the experimental observations.

VI. Conclusions

Dynamical instabilities in autoignition combustion are investigated by analyzing experimental data and low-order models. A two-state model, capturing the dynamics of the recycled thermal energy in the residual gases and the recycled chemical energy in the unburned fuel, is derived. Preliminary tuning of the model shows good agreement as dilution varies at one operating condition. Future work will aim for a systematic tuning methodology. The dynamical properties of the model are studied through bifurcation analysis and by adding stochastic noise, with properties estimated from data, to the bifurcation parameter which is the residual gas fraction. It is demonstrated that the onset of instability is predicted by the bifurcation analysis without noise and that the characteristics of the dynamical evolution seen at late phasing in experiments are reproduced by modeling the residual gas fraction as a Gaussian white noise process.

Acknowledgments

For helpful discussions on cyclic variability, we thank C. Stuart Daw at Oak Ridge National Laboratory and John W. Hoard at the University of Michigan. E. Hellström also gratefully acknowledges the award from Bernt Järmark's Foundation for Scientific Research.

This material is based upon work supported by the Department of Energy[1] and performed as a part of the ACCESS project consortium (Robert Bosch LLC, AVL Inc., Emitec Inc.) under the direction of PI Hakan Yilmaz, Robert Bosch, LLC.

[1]Disclaimer: This report was prepared as an account of work sponsored by an agency of the United States Government. Neither the United States Government nor any agency thereof, nor any of their employees, makes any warranty, express or implied, or assumes any legal liability or responsibility for the accuracy, completeness, or usefulness of any information, apparatus, product, or process disclosed, or represents that its use would not infringe privately owned rights. Reference herein to any specific commercial product, process, or service by trade name, trademark, manufacturer, or otherwise does not necessarily constitute or imply its endorsement, recommendation, or favoring by the United States Government or any agency thereof. The views and opinions of authors expressed herein do not necessarily state or reflect those of the United States Government or any agency thereof.

References

[1] D. Law, D. Kemp, J. Allen, G. Kirkpatrick, and T. Copland, "Controlled combustion in an IC-engine with a fully variable valvetrain," in *SAE World Congress*, 2001, SAE 2001-01-0251.

[2] R. H. Thring, "Homogeneous charge compression ignition (HCCI) engines," in *SAE Int. Fall Fuels and Lubricants Meeting and Exhibition*, 1989, SAE 892068.

[3] L. Koopmans and I. Denbratt, "A four stroke camless engine, operated in homogeneous charge compression ignition mode with commercial gasoline," in *SAE World Congress*, 2001, SAE 2001-01-3610.

[4] E. Hellström, A. G. Stefanopoulou, J. Vávra, A. Babajimopoulos, D. Assanis, L. Jiang, and H. Yilmaz, "Understanding the dynamic evolution of cyclic variability at the operating limits of HCCI engines with negative valve overlap," *SAE Int. J. Engines*, vol. 5, no. 3, pp. 995–1008, 2012.

[5] J.-O. Olsson, P. Tunestål, B. Johansson, S. Fiveland, R. Agama, and M. Willi, "Compression ratio influence on maximum load of a natural gas fueled HCCI engine," in *SAE World Congress*, 2002, SAE 2002-01-0111.

[6] L. Koopmans, O. Backlund, and I. Denbratt, "Cycle to cycle variations: Their influence on cycle resolved gas temperature and unburned hydrocarbons from a camless gasoline compression ignition engine," in *SAE World Congress*, 2002, SAE 2002-01-0110.

[7] S. Karagiorgis, N. Collings, K. Glover, N. Coghlan, and A. Petridis, "Residual gas fraction measurement and estimation on a homogeneous charge compression ignition engine utilizing the negative valve overlap strategy," in *SAE World Congr.*, 2006, SAE 2006-01-3276.

[8] D. Blom, M. Karlsson, K. Ekholm, P. Tunestål, and R. Johansson, "HCCI engine modeling and control using conservation principles," in *SAE World Congress*, 2008, SAE 2008-01-0789.

[9] R. M. Wagner, K. D. Edwards, C. S. Daw, J. B. Green, Jr., and B. G. Bunting, "On the nature of cyclic dispersion in spark assisted HCCI combustion," in *SAE World Congress*, 2006, SAE 2006-01-0418.

[10] J. Larimore, E. Hellström, J. Sterniak, L. Jiang, and A. G. Stefanopoulou, "Experiments and analysis of high cyclic variability at the operational limits of spark-assisted HCCI combustion," in *Proc. American Control Conference*, 2012, pp. 2072–2077.

[11] A. Ghazimirsaied, M. Shahbakhti, and C. R. Koch, "HCCI engine combustion phasing prediction using a symbolic-statistics approach," *J. Eng. Gas Turbines Power*, vol. 132, no. 8, p. 082805, 2010.

[12] G. M. Shaver and J. C. Gerdes, "Cycle-to-cycle control of HCCI engines," in *ASME Int. Mechanical Engineering Congress and Exposition*, 2003, iMECE 2003-41966.

[13] D. Rausen, A. Stefanopoulou, J.-M. Kang, E. J.A., and T.-W. Kuo, "A mean-value model for control of homogeneous charge compression ignition (HCCI) engines," *J. Dyn. Syst. Meas. Contr.*, vol. 3, no. 3, pp. 355–362, September 2005.

[14] A. Widd, P. Tunestål, and R. Johansson, "Physical modeling and control of homogeneous charge compression ignition (HCCI) engines," in *Proc. of the 47th IEEE Conference on Decision and Control*, 2008, pp. 5615–5620.

[15] C. J. Chiang, A. G. Stefanopoulou, and M. Jankovic, "Nonlinear observer-based control of load transitions in homogeneous charge compression ignition engines," *IEEE Trans. Control Syst. Technol.*, vol. 15, no. 3, pp. 438–448, May 2007.

[16] C. J. Chiang and A. G. Stefanopoulou, "Stability analysis in homogeneous charge compression ignition (HCCI) engines with high dilution," *IEEE Trans. Control Syst. Technol.*, vol. 15, no. 2, pp. 209–219, March 2007.

[17] J.-M. Kang, "Sensitivity analysis of auto-ignited combustion in HCCI engines," in *SAE World Congress*, 2010, SAE 2010-01-0573.

[18] H.-H. Liao, N. Ravi, A. F. Jungkunz, and J. C. Gerdes, "Representing recompression HCCI dynamics with a switching linear model," in *Proc. of the American Control Conference*, Baltimore, MD, USA, 2010, pp. 3803–3808.

[19] H. Song, A. Padmanabhan, N. B. Kaahaaina, and C. Edwards, "Experimental study of recompression reaction for low-load operation in direct-injection homogeneous charge compression ignition engines with n-heptane and i-octane fuels," *Int. J. Engine Res.*, vol. 10, no. 4, pp. 215–229, 2009.

[20] N. Wermuth, H. Yun, and P. Najt, "Enhancing light load HCCI combustion in a direct injection gasoline engine by fuel reforming during recompression," *SAE Int. J. Engines*, vol. 2, no. 1, pp. 823–836, 2009.

[21] N. Ravi, M. J. Roelle, H.-H. Liao, A. F. Jungkunz, C.-F. Chang, S. Park, and J. C. Gerdes, "Model-based control of HCCI engines using exhaust recompression," *IEEE Trans. Control Syst. Technol.*, vol. 18, no. 6, pp. 1289 –1302, 2010.

[22] A. F. Jungkunz, H.-H. Liao, N. Ravi, and J. C. Gerdes, "Reducing combustion variation of late-phasing HCCI with cycle-to-cycle exhaust valve timing control," in *IFAC Symp. on Advances in Automotive Control*, 2010.

[23] ——, "Combustion phasing variation reduction for late-phasing HCCI through cycle-to-cycle pilot injection timing control," in *Proc. of the ASME Dynamic Systems and Control Conference*, 2011.

[24] E. Hellström, J. Larimore, A. G. Stefanopoulou, J. Sterniak, and L. Jiang, "Quantifying cyclic variability in a multicylinder HCCI engine with high residuals," *J. Eng. Gas Turbines Power*, to appear.

[25] E. Hellström and A. G. Stefanopoulou, "Modeling cyclic dispersion in autoignition combustion," in *Proc. of the 50th IEEE Conference on Decision and Control*, 2011, pp. 6834–6839.

[26] K. L. Knierim, S. Park, J. Ahmed, A. Kojic, I. Orlandini, and A. Kulzer, "Simulation of misfire and strategies for misfire recovery of gasoline HCCI," in *Proc. of the American Control Conference*, 2008, pp. 3947–3952.

[27] C. G. Mayhew, K. L. Knierim, N. A. Chaturvedi, S. Park, J. Ahmed, and A. Kojic, "Reduced-order modeling for studying and controlling misfire in four-stroke HCCI engines," in *Proc. of the 48th IEEE Conference on Decision and Control*, 2009, pp. 5194–5199.

[28] J. C. Kantor, "A dynamical instability of spark-ignited engines," *Science*, vol. 224, no. 4654, pp. 1233–1235, 1984.

[29] C. S. Daw, M. B. Kennel, C. E. A. Finney, and F. T. Connolly, "Observing and modeling nonlinear dynamics in an internal combustion engine," *Phys. Rev. E*, vol. 57, no. 3, pp. 2811–2819, 1998.

[30] J. Willand, R.-G. Nieberding, G. Vent, and C. Enderle, "The knocking syndrome–its cure and its potential," in *SAE Int. Fall Fuels and Lubricants Meeting and Exhibition*, 1998, SAE 982483.

[31] J. Bengtsson, P. Strandh, R. Johansson, P. Tunestål, and B. Johansson, "Closed-loop combustion control of homogeneous charge compression ignition (HCCI) engine dynamics," *Int. J. Adapt Control Signal Process.*, vol. 18, no. 2, pp. 167–179, 2004.

[32] F. Agrell, H.-E. Ångström, B. Eriksson, J. Wikander, and J. Linderyd, "Integrated simulation and engine test of closed loop HCCI control by aid of variable valve timings," in *SAE World Congress*, 2003, SAE 2003-01-0748.

[33] J. C. Livengood and P. C. Wu, "Correlation of autoignition phenomena in internal combustion engines and rapid compression machines," in *5th Int. Symp. on Combustion*, vol. 5, no. 1, 1955, pp. 347–356.

[34] C. Daw, K. Edwards, R. Wagner, and J. B. Green, Jr., "Modeling cyclic variability in spark-assisted HCCI," *J. Eng. Gas Turbines Power*, vol. 130, no. 5, p. 052801, 2008.

[35] L. Manofsky, J. Vavra, D. Assanis, and A. Babajimopoulos, "Bridging the gap between HCCI and SI: Spark-assisted compression ignition," in *SAE World Congress*, 2011, SAE 2011-01-1179.

[36] J. Heywood, *Internal Combustion Engine Fundamentals*. McGraw-Hill, 1988.

[37] G. Weiss, "Time-reversibility of linear stochastic processes," *J. Appl. Probab.*, vol. 12, no. 4, pp. 831–836, 1975.

[38] Y. A. Kuznetsov, *Elements of Applied Bifurcation Theory*, 2nd ed. New York, NY, USA: Springer-Verlag, 1998.

[39] S. Wiggins, *Introduction to applied nonlinear dynamical systems and chaos*. New York, NY, USA: Springer-Verlag, 1990.